IEEE Access
Multidisciplinary | Rapid Review | Open Access Journal

SPECIAL SECTION ON ADVANCES IN SIGNAL PROCESSING FOR NON-ORTHOGONAL MULTIPLE ACCESS

Received June 13, 2019, accepted July 4, 2019, date of publication July 15, 2019, date of current version August 5, 2019.

Digital Object Identifier 10.1109/ACCESS.2019.2928877

An Efficient Design for NOMA-Assisted MISO-SWIPT Systems with AC Computing

VAN-DINH NGUYEN[1], (Student Member, IEEE), AND OH-SOON SHIN[1,2], (Member, IEEE)
[1]Department of ICMC Convergence Technology, Soongsil University, Seoul 06978, South Korea
[2]School of Electronic Engineering, Soongsil University, Seoul 06978, South Korea

Corresponding author: Oh-Soon Shin (osshin@ssu.ac.kr)

This work was supported by the Basic Science Research Program through the National Research Foundation of Korea (NRF) funded by the Ministry of Science and ICT under Grant NRF-2017R1A5A1015596.

ABSTRACT We consider a multiple-input single-output simultaneous wireless information and power transfer (MISO-SWIPT) system, where a power-splitting protocol is employed at users near the base station (BS) to provide both energy harvesting (EH) and information decoding. For the considered system, it is of practical interest to adopt non-orthogonal multiple access (NOMA) to improve the network spectral efficiency, while still meeting the EH requirements. In addition, an alternating current computing (ACC) logic is incorporated into EH receivers to directly use the wirelessly harvested AC power, which in turn achieves higher energy efficiency than traditional direct current computing (DCC). We formulate a problem of maximizing the spectral efficiency subject to the constraints of quality-of-service for the individual user, EH requirements, and BS's maximum transmit power, where the beamformers and PS ratios are jointly optimized. To achieve an efficient solution to this nonconvex problem, we propose an iterative algorithm based on the inner approximation (IA) framework, where the approximate convex problem solved in each iteration can be cast as a second-order-cone program with convergence guaranteed. To further simplify the problem design, we propose a zero-forcing beamforming-based NOMA approach to partially eliminate interference, which has the potential to significantly reduce the number of variables. The extensive numerical results are presented to demonstrate the effectiveness of the proposed algorithms, compared with the baseline schemes.

INDEX TERMS Alternating current computing (ACC), inner approximation, nonlinear energy harvesting, non-orthogonal multiple access (NOMA), nonconvex optimization, simultaneous wireless information and power transfer (SWIPT).

I. INTRODUCTION

The fifth generation (5G) wireless network has been recognized as the panacea of the current wireless networks to meet a dramatic growth of wireless devices, new applications and demand for wireless data traffic [1]. Accordingly, the total sum rate (SR) will certainly be considered as an important design objective for innovative wireless communication techniques. However, one of the most challenging tasks in the SR maximization problem is to guarantee the quality-of-service (QoS) in terms of data rate to users with poor channel condition, who are usually placed at the cell edge. In recent years, non-orthogonal multiple access (NOMA) technique is envisaged as a paradigm shift for the design of multiple access techniques to address this challenge [2]–[4].

Unlike with the traditional OMA techniques such as time-division multiple access, NOMA aims at serving multiple users on the same time-frequency resource and allocating different power levels to them.[1] In the scenario of two users [5], the user with poorer channel condition is generally allocated higher transmission power than the user with better channel condition to improve the edge data rate, while the latter is capable of canceling the interference from the former by successive interference cancellation (SIC) technique. When multiple users have similar channel conditions, dynamic user pairing and clustering with distinct channel gains are effective ways to exploit the potential of NOMA in providing the massive connectivity requirement of 5G networks [6]–[9].

The associate editor coordinating the review of this manuscript and approving it for publication was Zhiguo Ding.

[1]In this paper, we only focus on the power domain-based NOMA.

Simultaneous wireless information and power transfer (SWIPT) has been received growing attention recently [10], [11]. It utilizes radio frequency (RF) signals to realize both wireless energy harvesting (EH) and information decoding (ID). A SWIPT user splits the received signal into ID and EH receivers either by power splitting (PS) and time switching (TS) protocols, where the former has been shown to outperform the latter. EH receivers can be charged by converting the wirelessly harvested alternating current (AC) power into the direct current (DC) power, and its operation time is then prolonged [12]. Accordingly, the conversion efficiency plays an important role for efficient designs of diode-based RF-EH circuits, and recent experiments for practical EH models have shown that its characteristic is non-linear rather than linear [13], [14]. SWIPT systems [15]–[17] adopted traditional linear EH model which may result in inaccurate DC output, leading to significant system performance loss in practical implementations. Hence, non-linear EH models capturing non-linear characteristics have been intensively investigated [18]–[20].

A. LITERATURE SURVEY

Beamforming design is an effective way to improve the performance of multi-user NOMA systems. Reference [21] first studied the beamforming power minimization problem for the multiple-input single-output (MISO) system with two users, and a heuristic computational algorithm was proposed for its solution. In the case where there are multiple users, the power minimization problem is decomposed into the independent subproblems of two-user pairs by using zero-forcing beamformer (ZFBF) to remove the inter-pair interference. Chen *et al.* [22], [23] aimed at minimizing the beamforming power under users' QoS requirements, where the closed-form solutions were obtained. Reference [24] successively performed SIC at all users based on their channel gain differences, which may cause severe resource allocation mismatches. The authors in [6] and [7] proposed a simple but efficient design for NOMA systems by pairing one near user with one far user, where the cell coverage is divided into two zones with respect to the distance from the base station (BS). In general, the optimization problems for NOMA systems are nonconvex, and thus these works have mainly focused on suboptimal solutions.

NOMA aims at allocating high transmission power to far users, which in turn causes a strong interference to near users. This strong network interference has a great potential to boost the harvested energy for nearly-located users. Thus, NOMA-assisted SWIPT systems have received considerable attention. In particular, [25] investigated a joint optimization of power allocation and TS ratio to maximize the total energy efficiency (EE) in a TS-based SWIPT NOMA system subject to minimum users' harvested energy requirements. A trade-off between spectral efficiency and energy efficiency was studied in [26] by integrating SWIPT into mmWave massive multiple-input multiple-output (MIMO) NOMA systems. The work analyzed the impacts of the cluster-head selection algorithm, user pairing and hybrid precoding on the network performance. References [27] and [28] considered joint beamforming and PS design, where a strong user adopts the PS protocol and acts as an EH relay to retransmit the signal to the weak user. To further improve the network performance, the authors in [29] proposed a cooperative SWIPT NOMA system, where the full-duplex radio is enabled at a strong user.

Unfortunately, the aforementioned works have not taken into account the power consumption for activating the basic functions (i.e., computational blocks), especially at NOMA users, although they often require additional computational complexity due to the use of SIC. Given that the RF-EH performance is relatively low, the conventional methods that rely on DC computing (DCC) could lead to significant system performance loss due to low conversion efficiency of current rectifiers. To overcome this challenge, the authors in [30]–[32] have reported that the wirelessly harvested AC power can be directly used to activate computational blocks through practical experiments. The significant improvement in energy efficiency has been attained thanks to low-power consumption of AC computing (ACC) and no RF-EH conversion loss. The SR problems for NOMA-assisted MISO-SWIPT systems have remained relatively open in the literature to the best of our knowledge, in particular, new challenges will arise for the joint optimization of beamforming vectors and PS ratios.

B. CONTRIBUTIONS

Motivated by the literature survey and above discussion, in this work, we study the NOMA-assisted MISO-SWIPT system to realize both wireless EH and ID. Particularly, PS protocol is adopted at the nearly-located users (ID-EH users) to achieve SWIPT by splitting the received RF signals into two parts for simultaneous information and energy reception. To achieve energy-efficient design, we propose to integrate ACC logic into ID-EH users by leveraging charge-recycling theory to directly use the harvested AC power for computation. The goal is to maximize the total SR subject to power constraint and EH constraints at ID-EH users. Towards a relatively realistic model, we take into account the practical non-linear EH model and detection threshold for SIC receivers. Specifically, the contributions of this paper can be summarized as follows.

- First, we propose a new PS and SIC-based architecture which enables ACC for NOMA-SWIPT systems.
- We formulate a novel optimization problem to maximize the SR by jointly optimizing beamforming vectors and PS ratios. As the problem is highly nonconvex, we develop a low-complexity iterative algorithm based on the inner approximation (IA) framework for its solution with convergence guaranteed. The approximate problem at each iteration can be transformed into the second-order-cone program (SOCP) for efficient and practical implementation.

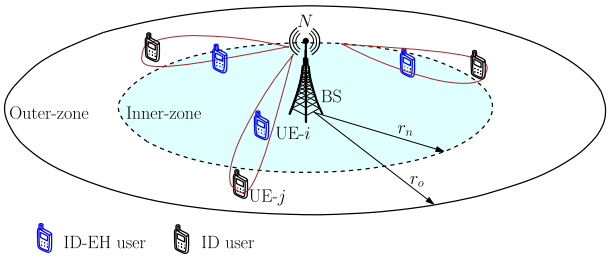

FIGURE 1. An illustration of the downlink NOMA-assisted MISO-SWIPT system serving multiple ID-EH and ID users.

- In addition, we develop a lower complexity solution based on the combination of ZFBF-NOMA and IA, which requires lower numbers of optimization variables.
- Extensive numerical results are provided to confirm the efficacy of our proposed approach. Specifically, the proposed resource allocation schemes achieve a significantly higher system performance compared to baseline schemes, i.e., conventional SWIPT, equal PS ratios and DCC-based design.

C. PAPER ORGANIZATION AND NOTATION

Organization: The remainder of the paper is organized as follows. Section II introduces the system model and formulates the optimization problem. In Section III, we present the IA-based algorithm. The problem design for ZFBF-NOMA and the proposed resource allocation algorithm based on IA method are provided in Section IV. Section V discusses the convergence and computational complexity of the proposed algorithms. Numerical results are presented in Section VI, and Section VII concludes the paper.

Notation: $\mathbf{x}^H$, $\mathbf{x}^T$, and $\mathbf{x}^*$ are the Hermitian transpose, normal transpose, and conjugate of a vector $\mathbf{x}$, respectively. $\mathbb{E}\{\cdot\}$ and $\Re\{\cdot\}$ denote the expectation and the real part of argument, respectively. $\|\cdot\|$ and $|\cdot|$ represent the ℓ_2 norm and absolute value, respectively. $\mathbb{R}^{n\times m}$ and $\mathbb{C}^{n\times m}$ are the vector space of real and complex matrices, respectively. $\mathbf{x} \sim \mathcal{CN}(\boldsymbol{\eta}, \boldsymbol{R})$ implies that $\mathbf{x}$ is a random vector following a circularly symmetric complex Gaussian distribution with mean vector $\boldsymbol{\eta}$ and covariance matrix $\boldsymbol{R}$.

II. SYSTEM MODEL AND PROBLEM STATEMENT

A. SIGNAL MODEL AND SYSTEM DESIGN

A downlink NOMA-assisted MISO-SWIPT system is considered, where the centered BS is equipped with N antennas to serve the set $\mathcal{K} \triangleq \{1, 2, \cdots, 2K\}$ of $2K = |\mathcal{K}|$ single-antenna users (UEs) on the same time-frequency resource, as illustrated in Fig. 1. Following [6], [7], [33], we assume that the whole cell is virtually divided into two zones, called inner-zone with radius r_n from the BS and outer-zone with inner radius r_n and outer radius r_o. Without loss of generality, we also assume that the system includes the set $\mathcal{K}_{\mathrm{I}} \triangleq \{1, \cdots, i, \cdots, K\}$ of $K = |\mathcal{K}_{\mathrm{I}}|$ near UEs which are randomly distributed in the inner-zone, as well as the other set $\mathcal{K}_{\mathrm{O}} \triangleq \{K+1, \cdots, j, \cdots, 2K\}$ of $K = |\mathcal{K}_{\mathrm{O}}|$ far UEs which are randomly distributed in the outer-zone. We note that the proposed algorithms in this paper can be slightly modified to address the case of different numbers of users located in each zone. It can be easily foreseen that UE-$i \in \mathcal{K}_{\mathrm{I}}$ has a better channel condition than UE-$j \in \mathcal{K}_{\mathrm{O}}$. In this paper, each near UE-i is randomly paired with far UE-j to create a virtual cluster, and SIC technique is used at UE-i, following the NOMA principle [6], [7]. The strong multiuser interference in the inner-zone offers great potential for UE-i to harvest the RF power. In what follows, UE-i and UE-j will be referred to as the ID-EH user and ID user, respectively.

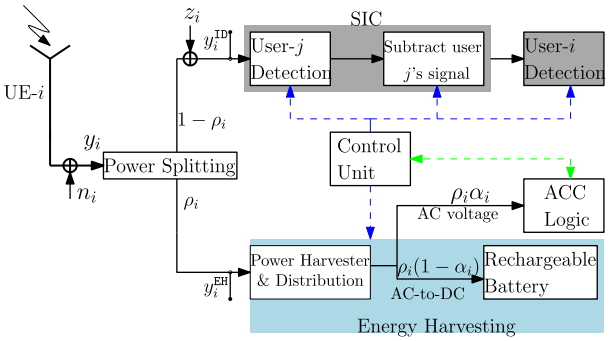

FIGURE 2. Power-splitting and SIC-based architecture enabled ACC at ID-EH user.

As shown in Fig. 2, we propose the PS and SIC-based architecture to perform SWIPT at UE-i (ID-EH user) using ACC logic. The received RF signal at UE-i is split into two parts, i.e., ID and EH signals. In the EH signal, the power harvester and distribution block is responsible for distributing the harvested AC power into two flows: one to directly supply the wirelessly harvested AC power for the ACC logic without rectification and regulation, and other to charge the battery for later use by using the AC-to-DC rectifier. In the conventional PS-based SWIPT designs (i.e., [10] and the references therein), DC computing often requires higher power consumption than ACC, which has been reported in [30], [32]. Otherwise, a power inverter to convey DC-to-AC voltage may be used to supply an AC voltage to the ACC logic, which results in the conversion loss of up to 10% $\sim$ 30% efficiency [34].

Remark 1: In this paper, to effectively convey the RF-EH power, we only consider the EH at users in the inner-zone. On the other hand, the ACC at near users is considered due to the following reason. The near users in the proposed NOMA-assisted MISO-SWIPT system need to handle higher computation tasks than far users due to the use of SIC, and thus, it is reasonable to directly use the harvested AC power which has the potential to significantly reduce the power consumption cost [32]. It is noted that the conversion efficiency of advanced rectifiers is relatively low, i.e., about 50% $\sim$ 60%.

The signals are linearly weighted with a complex vector at the BS prior to being transmitted to UEs. Specifically, BS transmits a signal superposition of the individual messages $\mathbf{w}_k x_k$ for $k \in \mathcal{K} \triangleq \mathcal{K}_{\mathrm{I}} \cup \mathcal{K}_{\mathrm{O}}$, where $\mathbf{w}_k \in \mathbb{C}^{N\times 1}$ and x_k with $\mathbb{E}\{|x_k|^2\} = 1$ are the beamformer and the

transmitted symbol for UE-k, respectively. The channels from the BS to UEs are supposed to be flat block-fading with the transmission block time T, which is normalized to 1 for notational simplicity. Let $\mathbf{h}_k \in \mathbb{C}^{N\times 1}$ denote the complex channel vector from the BS to UE-k. In addition, we assume that the channel state information is perfectly known at the BS [6], [7], [24], where the system optimization is carried out. Under flat fading channels, the received signal at UE-i (ID-EH user) is given by

$$y_i = \sum_{i'\in\mathcal{K}} \mathbf{h}_i^H \mathbf{w}_{i'} x_{i'} + n_i, \tag{1}$$

where $n_i \sim \mathcal{CN}(0, \sigma_i^2)$ is the antenna noise at UE-i which is modeled as the additive white Gaussian noise (AWGN). In Fig. 2, the received signal at UE-i is split into two parts by a power splitter, which are $\rho_i \in (0, 1)$ portion of y_i for the EH receiver and the remaining $(1-\rho_i)$ portion of y_i for the ID receiver. In particular, the signals received at the ID and EH receivers can be expressed as

$$y_i^{\mathrm{ID}} = (1-\rho_i)^{1/2}\Big(\mathbf{h}_i^H \mathbf{w}_i x_i + \mathbf{h}_i^H \mathbf{w}_j x_j + \sum_{i'\in\mathcal{K}\setminus\{i,j\}} \mathbf{h}_i^H \mathbf{w}_{i'} x_{i'} + n_i\Big) + z_i, \quad \forall i \in \mathcal{K}_{\mathrm{I}}, \tag{2}$$

$$y_i^{\mathrm{EH}} = \rho_i^{1/2}\Big(\sum_{k\in\mathcal{K}} \mathbf{h}_i^H \mathbf{w}_k x_k + n_i\Big), \quad \forall i \in \mathcal{K}_{\mathrm{I}}, \tag{3}$$

respectively. $z_i \sim \mathcal{CN}(0, \eta_i^2)$ denotes the additional circuit noise introduced by the ID receiver at UE-i, which is also modeled as the AWGN [15]. The signal received at UE-j, which is the ID user only, can be expressed as

$$y_j^{\mathrm{ID}} = \mathbf{h}_j^H \mathbf{w}_j x_j + \sum_{j'\in\mathcal{K}\setminus j} \mathbf{h}_j^H \mathbf{w}_{j'} x_{j'} + n_j. \quad \forall j \in \mathcal{K}_{\mathrm{O}}, \tag{4}$$

where $n_j \sim \mathcal{CN}(0, \sigma_j^2)$ is the AWGN at UE-j.

B. OPTIMIZATION PROBLEM FORMULATION

1) ACHIEVABLE RATE

In each pair of users, the symbol x_j of UE-j is decoded by both users, while the symbol x_i of UE-i is decoded by itself only after removing that of UE-j by the SIC. By defining $\mathbf{w} \triangleq \{\mathbf{w}_k\}_{k\in\mathcal{K}}$, the achievable rate (in nats/sec/Hz) by decoding x_j can be expressed as [7]

$$R_j(\mathbf{w}, \rho_i) = \log\Big(1 + \min\big(\gamma_j^j(\mathbf{w}), \gamma_j^i(\mathbf{w}, \rho_i)\big)\Big), \tag{5}$$

where

$$\gamma_j^j(\mathbf{w}) = \frac{|\mathbf{h}_j^H \mathbf{w}_j|^2}{\sum_{j'\in\mathcal{K}\setminus j} |\mathbf{h}_j^H \mathbf{w}_{j'}|^2 + \sigma_j^2} \tag{6}$$

is the signal-to-interference-plus-noise ratio (SINR) at UE-j in decoding its own symbol, and

$$\gamma_j^i(\mathbf{w}, \rho_i) = \frac{(1-\rho_i)|\mathbf{h}_i^H \mathbf{w}_j|^2}{(1-\rho_i)\Big(\sum_{i'\in\mathcal{K}\setminus j} |\mathbf{h}_i^H \mathbf{w}_{i'}|^2 + \sigma_i^2\Big) + \eta_i^2} = \frac{|\mathbf{h}_i^H \mathbf{w}_j|^2}{\sum_{i'\in\mathcal{K}\setminus j} |\mathbf{h}_i^H \mathbf{w}_{i'}|^2 + \sigma_i^2 + \frac{\eta_i^2}{1-\rho_i}} \tag{7}$$

is the SINR at UE-i in decoding the symbol x_j. Next, the achievable rate of UE-i by decoding its own symbol x_i after successfully canceling x_j is

$$R_i(\mathbf{w}, \rho_i) = \log\big(1 + \gamma_i(\mathbf{w}, \rho_i)\big), \tag{8}$$

with

$$\gamma_i(\mathbf{w}, \rho_i) = \frac{|\mathbf{h}_i^H \mathbf{w}_i|^2}{\sum_{i'\in\mathcal{K}\setminus\{i,j\}} |\mathbf{h}_i^H \mathbf{w}_{i'}|^2 + \sigma_i^2 + \frac{\eta_i^2}{1-\rho_i}}. \tag{9}$$

From (7) and (9), the following constraint in each pair of users also needs to be satisfied [9]:

$$|\mathbf{h}_i^H \mathbf{w}_j|^2 - |\mathbf{h}_i^H \mathbf{w}_i|^2 \geq P_{\mathrm{SIC}}, \quad \forall i, j, \tag{10}$$

where P_{SIC} is the minimum power difference required to distinguish between x_j and x_i at UE-i, which can be viewed as the detection threshold at the SIC receiver. This aims at guaranteeing an efficient SIC and avoiding a trivial data rate allocated to UE-j.

2) EH AND ACC POWER CONSUMPTION

In Fig. 2, let $\alpha_i \in (0, 1)$ be the fraction of harvested AC power at UE-i that is used to power the ACC logic. We assume that the power splitter at the power harvester and distribution block is perfect and induces no noise in the RF power. Thus, the harvested AC power at UE-i consumed by the ACC logic can be expressed as

$$p_i^{\mathrm{ACC}}(\mathbf{w}, \rho_i, \alpha_i) = \rho_i \alpha_i \sum_{k\in\mathcal{K}} |\mathbf{h}_i^H \mathbf{w}_k|^2, \tag{11}$$

where the noise power is ignored since it is negligible when compared to power transfer from the BS in practice. The remaining harvested AC power of UE-i is given as

$$p_i(\mathbf{w}, \rho_i, \alpha_i) = \rho_i(1-\alpha_i) \sum_{k\in\mathcal{K}} |\mathbf{h}_i^H \mathbf{w}_k|^2. \tag{12}$$

The rectifier converts $p_i(\mathbf{w}, \rho_i, \alpha_i)$ to DC power and stores it into its rechargeable battery. By considering a realistic RF-DC power rectifier in non-linear EH model [18], [19], the harvested DC power at UE-i is

$$p_i^{\mathrm{DC}}(\mathbf{w}, \rho_i, \alpha_i) = \frac{\bar{P}_i^{\mathrm{EH}}}{1-\Omega_i} \times \Big(\frac{1}{1+\exp\big(-a_i(p_i(\mathbf{w}, \rho_i, \alpha_i) - b_i)\big)} - \Omega_i\Big), \tag{13}$$

where $\bar{P}_i^{\mathrm{EH}}$ is the maximum power that can be harvested, a_i and b_i are constants depending on the circuit specifications, and $\Omega_i = \frac{1}{1+\exp(a_i b_i)}$.

Our goal is to maximize the total SR of all UEs subject to QoS for each UE, ACC power consumption and harvested DC power requirements at UE-i and power budget at the BS. Therefore, the optimization problem of interest with the ACC, denoted by SR-ACC for short, can be mathematically formulated as

$$\max_{\mathbf{w}, \boldsymbol{\rho}, \boldsymbol{\alpha}} \sum_{k\in\mathcal{K}} R_k(\mathbf{w}, \rho_i) \tag{14a}$$

$$\text{s.t. } R_k(\mathbf{w}, \rho_i) \geq \bar{R}_k, \quad \forall k \in \mathcal{K}, \tag{14b}$$
$$p_i^{\text{ACC}}(\mathbf{w}, \rho_i, \alpha_i) \geq \bar{P}_i^{\text{ACC}}, \quad \forall i \in \mathcal{K}_{\text{I}}, \tag{14c}$$
$$p_i^{\text{DC}}(\mathbf{w}, \rho_i, \alpha_i) \geq \bar{P}_i^{\text{DC}}, \quad \forall i \in \mathcal{K}_{\text{I}}, \tag{14d}$$
$$|\mathbf{h}_i^H \mathbf{w}_j|^2 - |\mathbf{h}_i^H \mathbf{w}_i|^2 \geq P_{\text{SIC}}, \quad \forall i, j, \tag{14e}$$
$$\rho_i \in (0, 1), \ \alpha_i \in (0, 1), \quad \forall i \in \mathcal{K}_{\text{I}}, \tag{14f}$$
$$\sum_{k \in \mathcal{K}} \|\mathbf{w}_k\|^2 \leq P_{\text{BS}}^{\max}, \tag{14g}$$

where $\boldsymbol{\rho} \triangleq \{\rho_i\}_{i \in \mathcal{K}_{\text{I}}}$ and $\boldsymbol{\alpha} \triangleq \{\alpha_i\}_{i \in \mathcal{K}_{\text{I}}}$. Constraint (14b) guarantees QoS for individual users, where $\bar{R}_k > 0$ is a predefined threshold. Constraints (14c) and (14d) are imposed to ensure that the ACC power consumption and harvested DC power at UE-i are larger than predefined thresholds, $\bar{P}_i^{\text{ACC}}$ and $\bar{P}_i^{\text{DC}}$, respectively. Constraint (14g) represents the transmit power constraint at the BS with the power budget $P_{\text{BS}}^{\max}$.

Remark 2: We note that, in DC computing, constraints (14c) and (14d) can be merged into one, such as

$$p_i^{\text{DC}}(\mathbf{w}, \rho_i, \alpha_i = 0) \geq \bar{P}_i^{\text{DCC}} + \bar{P}_i^{\text{DC}}, \quad \forall i \in \mathcal{K}_{\text{I}}, \tag{15}$$

where $\bar{P}_i^{\text{DCC}}$ is the DC power supply threshold that is required for the DCC logic. As previously mentioned, $\bar{P}_i^{\text{DCC}}$ is usually required to be much higher than $\bar{P}_i^{\text{ACC}}$ in practice. In addition, the conversion efficiency of an RF-DC power rectifier is typically low, thereby reducing the EH performance. These observations reveal the advantages of our proposed design, which will be elaborated by numerical results in Section VI.

Remark 3: In general, the optimal user-pairing schemes may improve the performance of NOMA-assisted MISO-SWIPT systems. However, as numerically demonstrated in Section VI, the SR achieved by our approach also catches up that by the Brute-Force Search (BFS) scheme, especially when the harvested DC power is high enough. In addition, the latter requires to solve $K!$ subproblems, each has the same form as in (14). As a result, the BFS scheme takes the complexity of $K!\mathcal{C}_{(14)}$, where $\mathcal{C}_{(14)}$ denotes the complexity of solving (14). It is prohibitive time complexity, and thus only acts as an upper bound of the performance of our proposed scheme.

In the following, we assume that the feasible set of problem (14) is nonempty. Finding an optimal solution to (14) is highly challenging due to the non-concavity of the objective (14a) and non-convexity of constraints (14b)-(14e). Although a globally optimal solution to (14) can be found through the Branch-and-Bound method, it is of little practical use in wireless communication designs since the channel conditions may vary quickly. In this work, by leveraging the IA framework, we propose an iterative low-complexity algorithm which aims at finding the approximate but efficient solution to (14).

III. PROPOSED IA-BASED ALGORITHM

The idea of the proposed IA-based algorithm is to transform (14) into an equivalent nonconvex, but more tractable, formulation and then apply the IA method to iteratively approximate the nonconvex parts to the convex ones [35], [36].

A. SOME IA-BASED APPROXIMATE FUNCTIONS

Before proceeding further, we first provide some IA-based approximate functions which will be frequently used in this paper. A function $f^{\text{UB}}(\mathbf{x}, \bar{\mathbf{x}})$ is a convex majorant of a function $f(\mathbf{x}) : \mathbb{C}^n \to \mathbb{R}$ at a point $\bar{\mathbf{x}} \in \mathbf{dom}\ f$, if and only if the following conditions are satisfied:

$$f^{\text{UB}}(\mathbf{x}, \bar{\mathbf{x}}) \geq f(\mathbf{x}) \quad \& \quad f^{\text{UB}}(\bar{\mathbf{x}}, \bar{\mathbf{x}}) = f(\bar{\mathbf{x}}), \quad \& \quad \frac{\partial f^{\text{UB}}(\mathbf{x}, \bar{\mathbf{x}})}{\partial \mathbf{x}}\Big|_{\mathbf{x}=\bar{\mathbf{x}}} = \frac{\partial f(\mathbf{x})}{\partial \mathbf{x}}\Big|_{\mathbf{x}=\bar{\mathbf{x}}}, \tag{16}$$

$\forall \mathbf{x} \in \mathbf{dom}\ f$. Similarly, a concave minorant $f^{\text{LB}}(\mathbf{x}, \bar{\mathbf{x}})$ of $f(\mathbf{x})$ must satisfy the following conditions:

$$f^{\text{LB}}(\mathbf{x}, \bar{\mathbf{x}}) \leq f(\mathbf{x}) \quad \& \quad f^{\text{LB}}(\bar{\mathbf{x}}, \bar{\mathbf{x}}) = f(\bar{\mathbf{x}}), \quad \& \quad \frac{\partial f^{\text{LB}}(\mathbf{x}, \bar{\mathbf{x}})}{\partial \mathbf{x}}\Big|_{\mathbf{x}=\bar{\mathbf{x}}} = \frac{\partial f(\mathbf{x})}{\partial \mathbf{x}}\Big|_{\mathbf{x}=\bar{\mathbf{x}}}. \tag{17}$$

The following approximate functions will follow these principles.

1) *Approximation for function $\frac{1}{xy}$ with $(x, y) \in \mathbb{R}_{++}^2$:* A convex upper bound (convex majorant) of $\frac{1}{xy}$ can be found as [35]:
$$\frac{1}{xy} \leq 0.5\Big(\frac{c}{x^2} + \frac{1}{cy^2}\Big), \tag{18}$$
where $c \triangleq \frac{\bar{x}}{\bar{y}}$.

2) *Approximation for function $\frac{x^2}{y}$ with $x \in \mathbb{C}$, $y \in \mathbb{R}_{++}$:* A concave lower bound of convex function $\frac{x^2}{y}$ is given as [37]:
$$\frac{x^2}{y} \geq 2\frac{\bar{x}^* x}{\bar{y}} - \frac{|\bar{x}|^2}{\bar{y}^2} y. \tag{19}$$

3) *Approximation for function $\log(1 + x)$ with $x \in \mathbb{R}_{++}$* [7, Eq. (66)]: We first consider the convex function $\log(1 + \frac{1}{z})$ with $z \in \mathbb{R}_{++}$, where its concave lower bound based on the first-order Taylor series is $\log(1 + \frac{1}{z}) \geq \log(1 + \frac{1}{\bar{z}}) + \frac{1}{(1+\bar{z})} - \frac{1}{(\bar{z}^2+\bar{z})} z$. Making a change of variables as $x \to 1/z$ and $\bar{x} \to 1/\bar{z}$, we derive the following concave lower bound of $\log(1 + x)$:
$$\log(1 + x) \geq \log(1 + \bar{x}) + \frac{\bar{x}}{1 + \bar{x}} - \frac{\bar{x}^2}{1 + \bar{x}} \frac{1}{x}. \tag{20}$$

B. PROPOSED ALGORITHM

We now transform (14) into a more tractable form, so that the IA method can be directly applied to tackle the nonconvex parts. To overcome non-smooth and non-concavity of (14a), we introduce new variables $\boldsymbol{\vartheta} \triangleq \{\vartheta\}_{k \in \mathcal{K}}$ and $\mathbf{r} \triangleq \{r\}_{k \in \mathcal{K}}$ to rewrite (14) equivalently as

$$\max_{\mathbf{w}, \boldsymbol{\rho}, \boldsymbol{\alpha}, \boldsymbol{\vartheta}, \mathbf{r}} \sum_{k \in \mathcal{K}} r_k \tag{21a}$$
$$\text{s.t. } \gamma_i(\mathbf{w}, \rho_i) \geq \vartheta_i, \quad \forall i \in \mathcal{K}_{\text{I}}, \tag{21b}$$
$$\min\big(\gamma_j^j(\mathbf{w}), \gamma_j^i(\mathbf{w}, \rho_i)\big) \geq \vartheta_j, \quad \forall j \in \mathcal{K}_{\text{O}}, \tag{21c}$$
$$\log(1 + \vartheta_k) \geq r_k, \quad \forall k \in \mathcal{K}, \tag{21d}$$
$$r_k \geq \bar{R}_k, \quad \forall k \in \mathcal{K}, \tag{21e}$$
$$(14c), (14d), (14e), (14f), (14g). \tag{21f}$$

Constraints (21b)-(21d) must hold with equality at the optimum and constraint (14b) is re-expressed as the linear constraint (21e). Here, the nonconvex constraints include (21b), (21c), (14c), (14d) and (14e). Let $y^{(\kappa)}$ denote a feasible point of y at the κ-th iteration of an iterative algorithm. We now apply the approximations presented in Section III-A to approximate (21) to a convex problem.

Approximation of constraints (21b) *and* (21c)*:* Let us handle the nonconvexity of constraint (21b) first. Following [38], it is true that $|\mathbf{h}_k^H\mathbf{w}_k| = \mathbf{h}_k^H\bar{\mathbf{w}}_k = \Re\{\mathbf{h}_k^H\bar{\mathbf{w}}_k\} \geq 0$ and $|\mathbf{h}_{k'}^H\mathbf{w}_k| = |\mathbf{h}_{k'}^H\bar{\mathbf{w}}_k|$, for all $k' \neq k$ and $\bar{\mathbf{w}}_k = e^{-j\arg(\mathbf{h}_k^H\mathbf{w}_k)}\mathbf{w}_k$ with $j = \sqrt{-1}$. Thus, (21b) can be equivalently replaced by

$$\frac{(\Re\{\mathbf{h}_i^H\mathbf{w}_i\})^2}{\vartheta_i} \geq \sum_{i'\in\mathcal{K}\setminus\{i,j\}} |\mathbf{h}_i^H\mathbf{w}_{i'}|^2 + \sigma_i^2 + \frac{\eta_i^2}{1-\rho_i}, \quad \forall i \in \mathcal{K}_{\mathrm{I}}, \tag{22}$$

with an additional condition:

$$\Re\{\mathbf{h}_i^H\mathbf{w}_i\} \geq 0, \quad \forall i \in \mathcal{K}_{\mathrm{I}}. \tag{23}$$

Also, to reveal the hidden convexity of constraint (22), we introduce new variables $\hat{\boldsymbol{\rho}} \triangleq \{\hat{\rho}_i\}_{i\in\mathcal{K}_{\mathrm{I}}}$ to equivalently rewrite it as

$$(22) \Leftrightarrow \begin{cases} \dfrac{(\Re\{\mathbf{h}_i^H\mathbf{w}_i\})^2}{\vartheta_i} \geq \displaystyle\sum_{i'\in\mathcal{K}\setminus\{i,j\}} |\mathbf{h}_i^H\mathbf{w}_{i'}|^2 \\ \qquad\qquad + \sigma_i^2 + \eta_i^2\hat{\rho}_i, \quad \forall i \in \mathcal{K}_{\mathrm{I}}, & \text{(24a)} \\ 1 \leq (1-\rho_i)\hat{\rho}_i, \quad \forall i \in \mathcal{K}_{\mathrm{I}}, & \text{(24b)} \end{cases}$$

where constraint (24b) is convex and also SOC-representable. It is observed that the functions in both sides of (24a) are convex, leading to a direct application of the IA method. Specifically, constraint (24a) is iteratively approximated by (19) as

$$\phi_i^{(\kappa)}(\mathbf{w}_i, \vartheta_i) - \eta_i^2\hat{\rho}_i \geq \sum_{i'\in\mathcal{K}\setminus\{i,j\}} |\mathbf{h}_i^H\mathbf{w}_{i'}|^2 + \sigma_i^2, \quad \forall i, \tag{25}$$

which is convex constraint, where

$$\phi_i^{(\kappa)}(\mathbf{w}_i, \vartheta_i) \triangleq 2\frac{\Re\{\mathbf{h}_i^H\mathbf{w}_i^{(\kappa)}\}\Re\{\mathbf{h}_i^H\mathbf{w}_i\}}{\vartheta_i^{(\kappa)}} - \frac{(\Re\{\mathbf{h}_i^H\mathbf{w}_i^{(\kappa)}\})^2}{(\vartheta_i^{(\kappa)})^2}\vartheta_i$$

is the first-order approximation of $\frac{(\Re\{\mathbf{h}_i^H\mathbf{w}_i\})^2}{\vartheta_i}$ around the point $(\mathbf{w}_i^{(\kappa)}, \vartheta_i^{(\kappa)})$. Next, constraint (21c) is re-expressed as

$$(21c) \Leftrightarrow \begin{cases} \gamma_j^j(\mathbf{w}) \geq \vartheta_j, & \text{(26a)} \\ \gamma_j^i(\mathbf{w}, \rho_i)) \geq \vartheta_j. & \text{(26b)} \end{cases}$$

Following the same steps as (22)-(25), constraint (26) is iteratively convexified as

$$\phi_j^{j,(\kappa)}(\mathbf{w}_j, \vartheta_j) \geq \sum_{j'\in\mathcal{K}\setminus j} |\mathbf{h}_j^H\mathbf{w}_{j'}|^2 + \sigma_j^2, \quad \forall j, * \tag{27a}$$

$$\phi_j^{i,(\kappa)}(\mathbf{w}_j, \vartheta_j) - \eta_i^2\hat{\rho}_i \geq \sum_{i'\in\mathcal{K}\setminus j} |\mathbf{h}_i^H\mathbf{w}_{i'}|^2 + \sigma_i^2, \quad \forall j, * \tag{27b}$$

under (24b) and the following additional constraint:

$$\Re\{\mathbf{h}_j^H\mathbf{w}_j\} \geq 0, \quad \forall j, \tag{28}$$

where

$$\phi_j^{j,(\kappa)}(\mathbf{w}_j, \vartheta_j) \triangleq 2\frac{\Re\{\mathbf{h}_j^H\mathbf{w}_j^{(\kappa)}\}\Re\{\mathbf{h}_j^H\mathbf{w}_j\}}{\vartheta_j^{(\kappa)}} - \frac{(\Re\{\mathbf{h}_j^H\mathbf{w}_j^{(\kappa)}\})^2}{(\vartheta_j^{(\kappa)})^2}\vartheta_j,$$

$$\phi_j^{i,(\kappa)}(\mathbf{w}_j, \vartheta_j) \triangleq 2\frac{\Re\{\mathbf{h}_i^H\mathbf{w}_j^{(\kappa)}(\mathbf{h}_i^H\mathbf{w}_j)^*\}}{\vartheta_j^{(\kappa)}} - \frac{|\mathbf{h}_i^H\mathbf{w}_j^{(\kappa)}|^2}{(\vartheta_j^{(\kappa)})^2}\vartheta_j.$$

Approximation of constraints (14c)-(14e)*:* We first rewrite (14c) as

$$\sum_{k\in\mathcal{K}} |\mathbf{h}_i^H\mathbf{w}_k|^2 \geq \frac{1}{\rho_i\alpha_i}\bar{P}_i^{\mathrm{ACC}}, \quad \forall i \in \mathcal{K}_{\mathrm{I}}. \tag{29}$$

We can observe that the left-hand side of (29) is a convex function, which is useful to develop an approximation by (19). In addition, a convex upper bound of $\frac{1}{\rho_i\alpha_i}$ is easily found by (18). As a result, constraint (29) is innerly approximated as

$$\mathcal{P}_i^{(\kappa)}(\mathbf{w}) \geq 0.5\bar{P}_i^{\mathrm{ACC}}\Big(\frac{c_i}{\rho_i^2} + \frac{1}{c_i\alpha_i^2}\Big), \quad \forall i \in \mathcal{K}_{\mathrm{I}}, \tag{30}$$

where $\mathcal{P}_i^{(\kappa)}(\mathbf{w}) \triangleq \sum_{k\in\mathcal{K}}\big(2\Re\{\mathbf{h}_i^H\mathbf{w}_k^{(\kappa)}(\mathbf{h}_i^H\mathbf{w}_k)^*\} - |\mathbf{h}_i^H\mathbf{w}_k^{(\kappa)}|^2\big)$ and $c_i \triangleq \rho_i^{(\kappa)}/\alpha_i^{(\kappa)}$. We note that the approximate constraint (30) is convex and can also be cast as the following second-order cone (SOC) ones:

$$0.5\bar{P}_i^{\mathrm{ACC}}\Big(c_i\tilde{\rho}_i^2 + \frac{\tilde{\alpha}_i^2}{c_i}\Big) \leq \mathcal{P}_i^{(\kappa)}(\mathbf{w}), \quad \forall i \in \mathcal{K}_{\mathrm{I}}, \tag{31a}$$

$$1 \leq \tilde{\rho}_i\rho_i, \quad \forall i \in \mathcal{K}_{\mathrm{I}}, \tag{31b}$$

$$1 \leq \tilde{\alpha}_i\alpha_i, \quad \forall i \in \mathcal{K}_{\mathrm{I}}, \tag{31c}$$

where $\tilde{\rho}_i$ and $\tilde{\alpha}_i$ are additional slack variables. For constraint (14d), we transform it into the following tractable form:

$$\sum_{k\in\mathcal{K}} |\mathbf{h}_i^H\mathbf{w}_k|^2 \geq \frac{1}{\rho_i(1-\alpha_i)}\zeta_i^{\mathrm{DC}}, \quad \forall i \in \mathcal{K}_{\mathrm{I}}, \tag{32}$$

where $\zeta_i^{\mathrm{DC}} \triangleq b_i - \frac{1}{a_i}\ln\Big(\frac{(\bar{P}_i^{\mathrm{EH}} - \bar{P}_i^{\mathrm{DC}})(1-\Omega_i)}{\bar{P}_i^{\mathrm{DC}}(1-\Omega_i) + \Omega_i\bar{P}_i^{\mathrm{EH}}}\Big)$. Similarly to (14c), an inner approximation of (14d) is

$$\mathcal{P}_i^{(\kappa)}(\mathbf{w}) \geq 0.5\zeta_i^{\mathrm{DC}}\Big(\frac{\tilde{c}_i}{\rho_i^2} + \frac{1}{\tilde{c}_i(1-\alpha_i)^2}\Big), \quad \forall i \in \mathcal{K}_{\mathrm{I}}, \tag{33}$$

where $\tilde{c}_i \triangleq \rho_i^{(\kappa)}/(1-\alpha_i^{(\kappa)})$ and $\mathcal{P}_i^{(\kappa)}(\mathbf{w})$ is defined in (30). Finally, we can easily approximate constraint (14e) as

$$\mathcal{H}_i^{(\kappa)}(\mathbf{w}_j) \geq |\mathbf{h}_i^H\mathbf{w}_i|^2 + P_{\mathrm{SIC}}, \quad \forall i, j, \tag{34}$$

where $\mathcal{H}_i^{(\kappa)}(\mathbf{w}_j) \triangleq 2\Re\{\mathbf{h}_i^H\mathbf{w}_j^{(\kappa)}(\mathbf{h}_i^H\mathbf{w}_j)^*\} - |\mathbf{h}_i^H\mathbf{w}_j^{(\kappa)}|^2$.

Bearing all the above in mind, we solve the following convex problem of (14) at iteration $(\kappa+1)$:

$$\max_{\mathbf{w},\boldsymbol{\rho},\boldsymbol{\alpha},\boldsymbol{\vartheta},\mathbf{r},\hat{\boldsymbol{\rho}}} \sum_{k\in\mathcal{K}} r_k \tag{35a}$$

$$\text{s.t. } \log(1+\vartheta_k) \geq r_k, \quad \forall k \in \mathcal{K}, \tag{35b}$$

$$\text{(14f), (14g), (21e), (23), (24b),}$$
$$\text{(25), (27a), (28), (30), (33), (34),} \tag{35c}$$

which arrives at least at a local optimum.

Solving (14) *by an SOCP*: Problem (35) is considered as a generic convex problem due to the logarithmic functions in (35b). Although the solution to this problem can be efficiently found using modern solvers (i.e., MOSEK [39]), it is more computationally efficient to cast (35) as an SOCP [40]. We note that the objective is monotonic in its argument in problem (35), while all the constraints are linear and SOC-representable, except for (35b). We are now in a position to iteratively approximate (35b) by (20), which is given as

$$\log\big(1+\vartheta_k^{(\kappa)}\big)+\frac{\vartheta_k^{(\kappa)}}{1+\vartheta_k^{(\kappa)}}-\frac{(\vartheta_k^{(\kappa)})^2}{1+\vartheta_k^{(\kappa)}}\frac{1}{\vartheta_k}\geq r_k,\quad \forall k\in\mathcal{K}. \tag{36}$$

Thus, the SOCP to solve (14) can be written in a compact form as

$$\max_{\boldsymbol{\Phi},\mathbf{r},\hat{\boldsymbol{\rho}}}\quad \Big\{\mathcal{R}^{(\kappa)}\triangleq\sum_{k\in\mathcal{K}}r_k\Big|\text{s.t.}\{\boldsymbol{\Phi},\mathbf{r},\hat{\boldsymbol{\rho}}\}\in\mathcal{C}\Big\}, \tag{37}$$

where $\boldsymbol{\Phi}$ and $\mathcal{C}$ are defined by the set of updated variables and feasible set, respectively, as

$$\boldsymbol{\Phi}\triangleq\{\mathbf{w},\boldsymbol{\rho},\boldsymbol{\alpha},\boldsymbol{\vartheta}\},$$
$$\mathcal{C}\triangleq\big\{\{\boldsymbol{\Phi},\mathbf{r},\hat{\boldsymbol{\rho}}\}\big|\text{(14f), (14g), (21e), (23), (24b), (25), (27), (28), (30), (33), (34), (36)}\big\}.$$

Generating an Initial Feasible Point: The IA-based algorithm requires an initial feasible point of (21), denoted by $\boldsymbol{\Phi}^{(0)}$, to successfully initialize the computational procedure at the first iteration. A random method may take many iterations or even fail to find a feasible point of (21), which is mainly due to constraints (14c)-(14e) and (21e). Here, we provide an efficient method inspired by [7], [33], [37] by considering the following modified optimization problem of (21):

$$\max_{\mathbf{w},\boldsymbol{\rho},\boldsymbol{\alpha},\boldsymbol{\vartheta},\mathbf{r},\tilde{\psi}}\quad \tilde{\psi} \tag{39a}$$
$$\text{s.t. } r_k-\bar{R}_k\geq\tilde{\psi},\quad \forall k\in\mathcal{K}, \tag{39b}$$
$$p_i^{\text{ACC}}(\mathbf{w},\rho_i,\alpha_i)-\bar{P}_i^{\text{ACC}}\geq\tilde{\psi},\quad \forall i\in\mathcal{K}_{\text{I}}, \tag{39c}$$
$$p_i^{\text{DC}}(\mathbf{w},\rho_i,\alpha_i)-\bar{P}_i^{\text{DC}}\geq\tilde{\psi},\quad \forall i\in\mathcal{K}_{\text{I}}, \tag{39d}$$
$$|\mathbf{h}_i^H\mathbf{w}_j|^2-|\mathbf{h}_i^H\mathbf{w}_i|^2-P_{\text{SIC}}\geq\tilde{\psi},\quad \forall i,j, \tag{39e}$$
$$\text{(14f), (14g), (21b)} - \text{(21d)}, \tag{39f}$$

where $\tilde{\psi}$ is a slack variable. Intuitively, a feasible point of (21) is found if (39) is feasible and $\psi\geq 0$. We first randomly generate $\boldsymbol{\rho}^{(0)}\in(0,1)$, $\boldsymbol{\alpha}^{(0)}\in(0,1)$ and $\mathbf{w}^{(0)}\in\mathbb{C}$, then scale $\mathbf{w}^{(0)}$ to ensure that {(14g), (23), (28)} are satisfied. With $(\boldsymbol{\rho}^{(0)},\boldsymbol{\alpha}^{(0)},\mathbf{w}^{(0)})$, $\boldsymbol{\vartheta}^{(0)}$ is calculated by setting inequalities (21b) and (21c) to be equalities. Based on $\boldsymbol{\Phi}^{(0)}$ and (37), we successively solve the following approximate convex program:

$$\max_{\boldsymbol{\Phi},\mathbf{r},\hat{\boldsymbol{\rho}},\psi}\quad \Big\{\psi\Big|\text{s.t.}\{\boldsymbol{\Phi},\mathbf{r},\hat{\boldsymbol{\rho}},\psi\}\in\mathcal{C}_0\Big\}, \tag{40}$$

where

$$\mathcal{C}_0\triangleq\Big\{\{\boldsymbol{\Phi},\mathbf{r},\hat{\boldsymbol{\rho}},\psi\}\big|r_k-\bar{R}_k\geq\psi,\quad\forall k\in\mathcal{K},$$
$$\mathcal{P}_i^{(\kappa)}(\mathbf{w})-0.5\bar{P}_i^{\text{ACC}}\Big(\frac{c_i}{\rho_i^2}+\frac{1}{c_i\alpha_i^2}\Big)\geq\psi,\quad\forall i\in\mathcal{K}_{\text{I}},$$
$$\mathcal{P}_i^{(\kappa)}(\mathbf{w})-0.5\zeta_i^{\text{DC}}\Big(\frac{\tilde{c}_i}{\rho_i^2}+\frac{1}{\tilde{c}_i(1-\alpha_i)^2}\Big)\geq\psi,\quad\forall i\in\mathcal{K}_{\text{I}},$$
$$\mathcal{H}_i^{(\kappa)}(\mathbf{w}_j)-|\mathbf{h}_i^H\mathbf{w}_i|^2-P_{\text{SIC}}\geq\psi,\quad\forall i,j,$$
$$\text{(14f), (14g), (23), (24b), (25), (27a), (28), (36)}\Big\}.$$

We notice that any feasible point of (40) is also feasible to (39), following the IA properties [35]. Whenever (40) is successfully solved and $\psi\geq 0$, a feasible point of (21) is produced. In Algorithm 1, we summarize our proposed IA-based algorithm to solve the SR-ACC problem (14).

Algorithm 1 Proposed IA-Based Algorithm for Solving SR-ACC (14)

Initialization: Set $\kappa:=0$, $\kappa':=0$ and randomly generate a feasible initial point $\boldsymbol{\Phi}^{(0)}$ for (40).
Generating a feasible point for (21):
repeat
  Solve $\max_{\boldsymbol{\Phi},\mathbf{r},\hat{\boldsymbol{\rho}},\psi}\big\{\psi\big|\text{s.t.}\{\boldsymbol{\Phi},\mathbf{r},\hat{\boldsymbol{\rho}},\psi\}\in\mathcal{C}_0\big\}$ to obtain the optimal solution $\boldsymbol{\Phi}^\star$.
  Update $\boldsymbol{\Phi}^{(\kappa'+1)}:=\boldsymbol{\Phi}^\star$.
  Set $\kappa':=\kappa'+1$.
until $\psi\geq 0$
Set $\boldsymbol{\Phi}^{(0)}:=\boldsymbol{\Phi}^{(\kappa')}$.
Solving (21):
repeat
  Solve $\max_{\boldsymbol{\Phi},\mathbf{r},\hat{\boldsymbol{\rho}}}\big\{\mathcal{R}^{(\kappa)}\triangleq\sum_{k\in\mathcal{K}}r_k\big|\text{s.t.}\{\boldsymbol{\Phi},\mathbf{r},\hat{\boldsymbol{\rho}}\}\in\mathcal{C}\big\}$ to obtain the optimal solution $\boldsymbol{\Phi}^\star$.
  Update $\boldsymbol{\Phi}^{(\kappa+1)}:=\boldsymbol{\Phi}^\star$.
  Set $\kappa:=\kappa+1$.
until Convergence or $\frac{\mathcal{R}^{(\kappa)}-\mathcal{R}^{(\kappa-1)}}{\mathcal{R}^{(\kappa-1)}}\leq\epsilon$
Output: $(\mathbf{w},\boldsymbol{\rho},\boldsymbol{\alpha}):=(\mathbf{w}^{(\kappa)},\boldsymbol{\rho}^{(\kappa)},\boldsymbol{\alpha}^{(\kappa)})$.

IV. ZERO-FORCING BEAMFORMING-BASED NOMA DESIGN

To further reduce the complexity in solving (14), we now adopt the zero-forcing beamforming-based NOMA (ZFBF-NOMA) method to partially eliminate the inter-user interference, except for the signal of UE-j being decoded at UE-i, i.e., $\mathbf{h}_j^H\mathbf{w}_{j'}=0,\forall j'\neq j$ and $\mathbf{h}_i^H\mathbf{w}_{i'}=0,\forall i'\neq\{i,j\}$. For SR-ACC problem, using ZFBF-NOMA does not lead to a convex problem due to the complexity involved. However, we can arrive at a suboptimal solution but with much less complexity, following the similar method presented in Section III. Specifically, let us define $\mathbf{H}_i\triangleq[\mathbf{h}_1\cdots\mathbf{h}_{i-1}\quad\mathbf{h}_{i+1}\cdots\mathbf{h}_{2K}]^H\in\mathbb{C}^{(2K-1)\times N},\forall i\in\mathcal{K}_{\text{I}}$ and $\mathbf{H}_j\triangleq[\mathbf{h}_1\cdots\mathbf{h}_{i-1}\mathbf{h}_{i+1}\cdots\mathbf{h}_{j-1}\mathbf{h}_{j+1}\cdots\mathbf{h}_{2K}]^H\in\mathbb{C}^{(2K-2)\times N},\forall i\in\mathcal{K}_{\text{I}},j\in\mathcal{K}_{\text{O}}$. Let $\mathbf{T}_i\in\mathbb{C}^{N\times(N-2K+1)}$ and

$\mathbf{T}_j \in \mathbb{C}^{N\times(N-2K+2)}$ be orthonormal bases of the null-space of $\mathbf{H}_i$ and $\mathbf{H}_j$, respectively. In this paper, we assume that $N > 2K-1$ so that $\mathbf{T}_i$ and $\mathbf{T}_j$ exist. By the ZFBF-NOMA method, the beamformers can be re-expressed as [41]

$$\mathbf{w}_i = \mathbf{T}_i\tilde{\mathbf{w}}_i, \quad \forall i \in \mathcal{K}_{\mathrm{I}},$$
$$\mathbf{w}_j = \mathbf{T}_j\tilde{\mathbf{w}}_j, \quad \forall j \in \mathcal{K}_{\mathrm{O}},$$

where $\tilde{\mathbf{w}}_i \in \mathbb{C}^{(N-2K+1)\times 1}$ and $\tilde{\mathbf{w}}_j \in \mathbb{C}^{(N-2K+2)\times 1}$ are new decision variables.

The SR-ACC optimization problem with ZFBF-NOMA is modified to the following problem:

$$\max_{\tilde{\mathbf{w}},\boldsymbol{\rho},\boldsymbol{\alpha}} \sum_{k\in\mathcal{K}} R_k^{\mathrm{ZF}}(\tilde{\mathbf{w}}, \rho_i) \tag{42a}$$
$$\text{s.t. } R_k^{\mathrm{ZF}}(\tilde{\mathbf{w}}, \rho_i) \geq \bar{R}_k, \quad \forall k \in \mathcal{K}, \tag{42b}$$
$$p_i^{\mathrm{ACC,ZF}}(\tilde{\mathbf{w}}, \rho_i, \alpha_i) \geq \bar{P}_i^{\mathrm{ACC}}, \quad \forall i \in \mathcal{K}_{\mathrm{I}}, \tag{42c}$$
$$p_i^{\mathrm{DC,ZF}}(\tilde{\mathbf{w}}, \rho_i, \alpha_i) \geq \bar{P}_i^{\mathrm{DC}}, \quad \forall i \in \mathcal{K}_{\mathrm{I}}, \tag{42d}$$
$$|\tilde{\mathbf{h}}_i^H\tilde{\mathbf{w}}_j|^2 - |\tilde{\mathbf{h}}_i^H\tilde{\mathbf{w}}_i|^2 \geq P_{\mathrm{SIC}}, \quad \forall i,j, \tag{42e}$$
$$\sum_{k\in\mathcal{K}} \|\tilde{\mathbf{w}}_k\|^2 \leq P_{\mathrm{BS}}^{\max}, \tag{42f}$$
$$(14\mathrm{f}), \tag{42g}$$

where $\tilde{\mathbf{w}} \triangleq \{\{\tilde{\mathbf{w}}_i\}_{i\in\mathcal{K}_{\mathrm{I}}}, \{\tilde{\mathbf{w}}_j\}_{j\in\mathcal{K}_{\mathrm{O}}}\}$, $\tilde{\mathbf{h}}_i^H \triangleq \mathbf{h}_i^H\mathbf{T}_i \in \mathbb{C}^{1\times(N-2K+1)}$, $\tilde{\mathbf{h}}_j^H \triangleq \mathbf{h}_j^H\mathbf{T}_j \in \mathbb{C}^{1\times(N-2K+2)}$, and

$$R_j^{\mathrm{ZF}}(\tilde{\mathbf{w}}, \rho_i) = \log\Big(1+\min\big(\gamma_j^{j,\mathrm{ZF}}(\tilde{\mathbf{w}}), \gamma_j^{i,\mathrm{ZF}}(\tilde{\mathbf{w}}, \rho_i)\big)\Big),$$
$$R_i^{\mathrm{ZF}}(\tilde{\mathbf{w}}, \rho_i) = \log\big(1+\gamma_i^{\mathrm{ZF}}(\tilde{\mathbf{w}}, \rho_i)\big),$$
$$p_i^{\mathrm{ACC,ZF}}(\tilde{\mathbf{w}}, \rho_i, \alpha_i) = \rho_i\alpha_i \sum_{k'\in\{i,j\}} |\tilde{\mathbf{h}}_i^H\tilde{\mathbf{w}}_{k'}|^2,$$
$$p_i^{\mathrm{DC,ZF}}(\tilde{\mathbf{w}}, \rho_i, \alpha_i) = \frac{\bar{P}_i^{\mathrm{EH}}}{1-\Omega_i} \times\Big(\frac{1}{1+\exp\big(-a_i(p_i^{\mathrm{ZF}}(\tilde{\mathbf{w}}, \rho_i, \alpha_i)-b_i)\big)}-\Omega_i\Big),$$

with

$$\gamma_j^{j,\mathrm{ZF}}(\tilde{\mathbf{w}}) = \frac{|\tilde{\mathbf{h}}_j^H\tilde{\mathbf{w}}_j|^2}{\sigma_j^2},$$
$$\gamma_j^{i,\mathrm{ZF}}(\tilde{\mathbf{w}}, \rho_i) = \frac{|\tilde{\mathbf{h}}_i^H\tilde{\mathbf{w}}_j|^2}{|\tilde{\mathbf{h}}_i^H\tilde{\mathbf{w}}_i|^2 + \sigma_i^2 + \frac{\eta_i^2}{1-\rho_i}},$$
$$\gamma_i^{\mathrm{ZF}}(\tilde{\mathbf{w}}, \rho_i) = \frac{|\tilde{\mathbf{h}}_i^H\tilde{\mathbf{w}}_i|^2}{\sigma_i^2 + \frac{\eta_i^2}{1-\rho_i}},$$
$$p_i^{\mathrm{ZF}}(\tilde{\mathbf{w}}, \rho_i, \alpha_i) = \rho_i(1-\alpha_i) \sum_{k'\in\{i,j\}} |\tilde{\mathbf{h}}_i^H\tilde{\mathbf{w}}_{k'}|^2.$$

Under the similar developments presented in Section III, at iteration $(\kappa+1)$ we solve the following convex program, which can be transformed to an SOCP, to find a locally optimal solution to (42):

$$\max_{\tilde{\boldsymbol{\Phi}},\mathbf{r},\hat{\boldsymbol{\rho}}} \quad \Big\{\tilde{\mathcal{R}}^{(\kappa)} \triangleq \sum_{k\in\mathcal{K}} r_k \Big| \text{s.t.}\{\tilde{\boldsymbol{\Phi}}, \mathbf{r}, \hat{\boldsymbol{\rho}}\} \in \tilde{\mathcal{C}}\Big\}, \tag{45}$$

where $\tilde{\boldsymbol{\Phi}}$ and $\tilde{\mathcal{C}}$ are redefined as

$$\tilde{\boldsymbol{\Phi}} \triangleq \{\tilde{\mathbf{w}}, \boldsymbol{\rho}, \boldsymbol{\alpha}, \boldsymbol{\vartheta}\},$$
$$\tilde{\mathcal{C}} \triangleq \Big\{\{\tilde{\boldsymbol{\Phi}}, \mathbf{r}, \hat{\boldsymbol{\rho}}\} \Big| (14\mathrm{f}), (21\mathrm{e}), (24\mathrm{b}), (36), (42\mathrm{f}),$$
$$\Re\{\tilde{\mathbf{h}}_k^H\tilde{\mathbf{w}}_k\} \geq 0, \quad \forall k \in \mathcal{K},$$
$$\tilde{\phi}_i^{(\kappa)}(\tilde{\mathbf{w}}_i, \vartheta_i) \geq \sigma_i^2 + \eta_i^2\hat{\rho}_i, \quad \forall i,$$
$$\tilde{\phi}_j^{j,(\kappa)}(\tilde{\mathbf{w}}_j, \vartheta_j) \geq \sigma_j^2, \quad \forall j,$$
$$\tilde{\phi}_j^{i,(\kappa)}(\tilde{\mathbf{w}}_j, \vartheta_j) - \eta_i^2\hat{\rho}_i \geq |\tilde{\mathbf{h}}_i^H\tilde{\mathbf{w}}_i|^2 + \sigma_i^2, \quad \forall j,$$
$$\mathcal{P}_i^{\mathrm{ZF},(\kappa)}(\tilde{\mathbf{w}}) \geq 0.5\bar{P}_i^{\mathrm{ACC}}\Big(\frac{c_i}{\rho_i^2} + \frac{1}{c_i\alpha_i^2}\Big), \quad \forall i \in \mathcal{K}_{\mathrm{I}},$$
$$\mathcal{P}_i^{\mathrm{ZF},(\kappa)}(\tilde{\mathbf{w}}) \geq 0.5\zeta_i^{\mathrm{DC}}\Big(\frac{\tilde{c}_i}{\rho_i^2} + \frac{1}{\tilde{c}_i(1-\alpha_i)^2}\Big), \quad \forall i \in \mathcal{K}_{\mathrm{I}},$$
$$\mathcal{H}_i^{(\kappa)}(\tilde{\mathbf{w}}_j) \geq |\mathbf{h}_i^H\tilde{\mathbf{w}}_i|^2 + P_{\mathrm{SIC}}, \quad \forall i,j\Big\},$$

with

$$\tilde{\phi}_i^{(\kappa)}(\tilde{\mathbf{w}}_i, \vartheta_i) \triangleq 2\frac{\Re\{\tilde{\mathbf{h}}_i^H\tilde{\mathbf{w}}_i^{(\kappa)}\}\Re\{\tilde{\mathbf{h}}_i^H\tilde{\mathbf{w}}_i\}}{\vartheta_i^{(\kappa)}} - \frac{(\Re\{\tilde{\mathbf{h}}_i^H\tilde{\mathbf{w}}_i^{(\kappa)}\})^2}{(\vartheta_i^{(\kappa)})^2}\vartheta_i,$$
$$\tilde{\phi}_j^{j,(\kappa)}(\tilde{\mathbf{w}}_j, \vartheta_j) \triangleq 2\frac{\Re\{\tilde{\mathbf{h}}_j^H\tilde{\mathbf{w}}_j^{(\kappa)}\}\Re\{\tilde{\mathbf{h}}_j^H\tilde{\mathbf{w}}_j\}}{\vartheta_j^{(\kappa)}} - \frac{(\Re\{\tilde{\mathbf{h}}_j^H\tilde{\mathbf{w}}_j^{(\kappa)}\})^2}{(\vartheta_j^{(\kappa)})^2}\vartheta_j,$$
$$\tilde{\phi}_j^{i,(\kappa)}(\tilde{\mathbf{w}}_j, \vartheta_j) \triangleq 2\frac{\Re\{\tilde{\mathbf{h}}_i^H\tilde{\mathbf{w}}_j^{(\kappa)}(\tilde{\mathbf{h}}_i^H\tilde{\mathbf{w}}_j)^*\}}{\vartheta_j^{(\kappa)}} - \frac{|\tilde{\mathbf{h}}_i^H\tilde{\mathbf{w}}_j^{(\kappa)}|^2}{(\vartheta_j^{(\kappa)})^2}\vartheta_j,$$
$$\mathcal{P}_i^{\mathrm{ZF},(\kappa)}(\tilde{\mathbf{w}}) \triangleq \sum_{k'\in\{i,j\}} \big(2\Re\{\tilde{\mathbf{h}}_i^H\tilde{\mathbf{w}}_{k'}^{(\kappa)}(\tilde{\mathbf{h}}_i^H\tilde{\mathbf{w}}_{k'})^*\} - |\tilde{\mathbf{h}}_i^H\tilde{\mathbf{w}}_{k'}^{(\kappa)}|^2\big),$$
$$\mathcal{H}_i^{(\kappa)}(\tilde{\mathbf{w}}_j) \triangleq 2\Re\{\tilde{\mathbf{h}}_i^H\tilde{\mathbf{w}}_j^{(\kappa)}(\tilde{\mathbf{h}}_i^H\tilde{\mathbf{w}}_j)^*\} - |\tilde{\mathbf{h}}_i^H\tilde{\mathbf{w}}_j^{(\kappa)}|^2.$$

To solve problem (42), we customize Algorithm 1 as follows. In Step 2, we generate an initial feasible point using the similar procedure described in (40). In Step 8, we solve the SOCP (45) instead of (37). For the ease of exposition, we refer to this customized algorithm as Algorithm 2.

V. CONVERGENCE AND COMPUTATIONAL COMPLEXITY ANALYSIS

Convergence Analysis: The iterative procedure of Algorithms 1 and 2 provably converges to a Karush-Kuhn-Tucker (KKT) point of (14) and (42), respectively, which has been provided in [35]. Herein, we only briefly examine the necessary conditions to justify the convergence of the proposed algorithms. Specifically, the approximate functions in (37) and (45) satisfy (16) and (17), which also correspond to the properties listed in [36]. Since the feasible sets of the considered problems are compact and nonempty, Algorithms 1 and 2 generate a sequence of improved objective values, i.e., $\mathcal{R}^{(\kappa)} \geq \mathcal{R}^{(\kappa-1)}$ and $\tilde{\mathcal{R}}^{(\kappa)} \geq \tilde{\mathcal{R}}^{(\kappa-1)}$, that are monotonically convergent after a finite number of iterations [35]. In other words, the stationary points of Algorithms 1 and 2 achieve the necessary optimality conditions of the nonconvex problems (14) and (42), respectively.

TABLE 1. Simulation parameters.

Parameter	Value
Number of users, $2K$	6
QoS for individual users, $\bar{R} \equiv \bar{R}_k, \forall k \in \mathcal{K}$	0.5 bps/Hz
Harvested DC power requirement, $\bar{P}^{\mathrm{DC}} \equiv \bar{P}_i^{\mathrm{DC}}, \forall i \in \mathcal{K}_{\mathrm{I}}$	-20 dBm
ACC power consumption, $\bar{P}^{\mathrm{ACC}} \equiv \bar{P}_i^{\mathrm{ACC}}, \forall i \in \mathcal{K}_{\mathrm{I}}$ [32]	-35.68 dBm
DCC power consumption, $\bar{P}^{\mathrm{DCC}} \equiv \bar{P}_i^{\mathrm{DCC}}, \forall i \in \mathcal{K}_{\mathrm{I}}$ [32]	-13.22 dBm
Detection threshold for SIC, P_{SIC}	-50 dBm
Maximum EH power, $\bar{P}^{\mathrm{EH}} \equiv \bar{P}_i^{\mathrm{EH}}, \forall i \in \mathcal{K}_{\mathrm{I}}$ [19]	0.79 dBm
Circuit specifications of EH model, $(a_i, b_i, \forall i)$ [42]	(1500, 0.0022)
Variance of antenna noise, $\sigma^2 \equiv \sigma_k^2, \forall k \in \mathcal{K}$	-95 dBm
Variance of additional circuit noise, $\eta^2 \equiv \eta_i^2, \forall i \in \mathcal{K}_{\mathrm{I}}$	-80 dBm

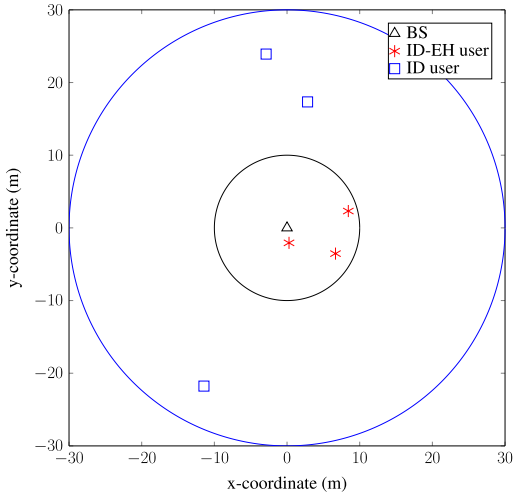

FIGURE 3. A small cell DL network topology with near-BS ID-EH users is used, where $r_n = 10$ m and $r_o = 30$ m. Three ID-EH users are randomly located in inner-zone with the reference distance of 2 m. Three ID users are randomly located in outer-zone.

Computational Complexity Analysis: We now discuss the per-iteration complexity of Algorithms 1 and 2 in solving the SOCP approximations (37) and (45), respectively, by the primal-dual interior point method [40]. Recall that N and $2K$ denote the number of antennas at the BS and the number of users, respectively. In Algorithm 1, problem (37) involves $K(2N + 7)$ scalar real decision variables and $(15K + 1)$ linear and SOC constraints, and thus the worst case of the per-iteration complexity required to solve (37) is $\mathcal{O}\Big((15K)^{0.5}\big(K(2N + 7)\big)^3\Big)$. In Algorithm 2, by using ZFBF-NOMA, the number of scalar real decision variables in the SOCP approximation (45) is reduced to $2K(N + 5 - 2K)$ and the number of constraints is $(15K + 1)$. The worst case of the per-iteration complexity for solving (45) is $\mathcal{O}\Big((15K)^{0.5}\big(2K(N+5-2K)\big)^3\Big)$, which is lower than that of Algorithm 1.

VI. NUMERICAL RESULTS

In this section, we evaluate the performance of the proposed methods using computer simulations. We consider the small cell DL network topology with $2K = 6$ users, as illustrated in Fig. 3. There are three ID-EH users and three ID users, which are randomly located in inner-zone and outer-zone, respectively. Here, the channel quality of ID-EH users is favored to better harvest energy. The channel vector between the BS and UE-k, $\forall k \in \mathcal{K}$ at the distance d_k (in meters) is generated as $\mathbf{h}_k = \sqrt{10^{-\mathsf{PL}_k/10}}\bar{\mathbf{h}}$, where $\mathsf{PL}_k = 30.18 + 26\log_{10}(d_k)$ (dB) is the path loss (PL) and $\bar{\mathbf{h}} \sim \mathcal{CN}(0, \mathbf{I})$ is the small-scale fading [43]. Unless stated otherwise, the simulation parameters are specified in Table 1, where we assume that users have the same set of parameters. The proposed algorithms are terminated when the error tolerance between two consecutive iterations is less than $\epsilon = 10^{-3}$. To arrive at units of bps/channel-use, we divide the achieved sum rate in nats/sec/Hz by ln(2). To solve the convex program, we use the toolbox YALMIP [44] with the SDPT3 solver [45] in the MATLAB environment. The average system performance is obtained by averaging over 1,000 independent channel realizations.

To demonstrate the effectiveness of the proposed methods with ACC, we reformulate (14) and (42) using DCC, i.e., by replacing constraints (14c) and (14d) with (15). The solutions for these problems can be easily found using Algorithms 1 and 2 after some slight modifications, which are referred to as "Algorithm 1 with DCC" and "Algorithm 2 with DCC", respectively. For benchmarking purpose, we also compare the performance of the proposed algorithms with that of the following three baseline schemes:

- "Brute-Force Search (BFS):" We consider an optimal user-pairing scheme based on the BFS method, which aims at finding the best user-pairing scheme among all $K!$ possibilities. This requires to solve $K!$ subproblems, and the optimal solution of the BFS method corresponds to the solution of the subproblem that provides the highest objective value. It is noted that problem (14) is a random case of the BFS, and thus each subproblem of the BFS-based scheme can be solved using Algorithm 1.
- "Without NOMA:" In this case, SIC technique is not used at UE-i, $\forall i \in \mathcal{K}_{\mathrm{I}}$, which aims to show the efficacy of NOMA transmission in enhancing system performance. The optimization problem can be easily derived from (14) by modifying SINRs at users and removing the SIC constraint (14e).
- "Equal Power-Splitting (EPS):" The power-splitting ratios are fixed to be $\rho_i = 0.5, \forall i \in \mathcal{K}_{\mathrm{I}}$, and the other optimization variables are found using the IA-based algorithm similar to Algorithm 1.

Fig. 4 illustrates the typical convergence behavior of the proposed algorithms over a random channel with $N = 8$ and $P_{\mathrm{BS}}^{\max} = 42$ dBm. Performances with DCC are also plotted. It can be seen that Algorithm 1 converges with tens of iterations in both ACC and DCC. We also see in the figure that with the ZFBF, Algorithm 2 converges with much fewer iterations compared to Algorithm 1. More importantly, the results clearly demonstrate that using the ACC logic for the considered problems provides much better performance than that of the DCC one in terms of SR. The reasons are twofold: *i*) ACC logic consumes much less power than DCC one, i.e., -35.68 dBm and -13.22 dBm, respectively, following the measurement data from [32, Fig. 6]; *ii*) Due to limited harvested power, the conversion loss of AC-to-DC rectifier

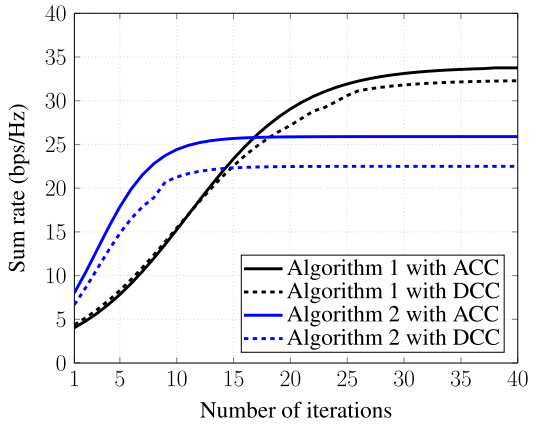

FIGURE 4. Convergence behavior of the proposed algorithms with ACC and DCC over one random channel realization with $N = 8$ and $P_{\mathrm{BS}}^{\max} = 42$ dBm.

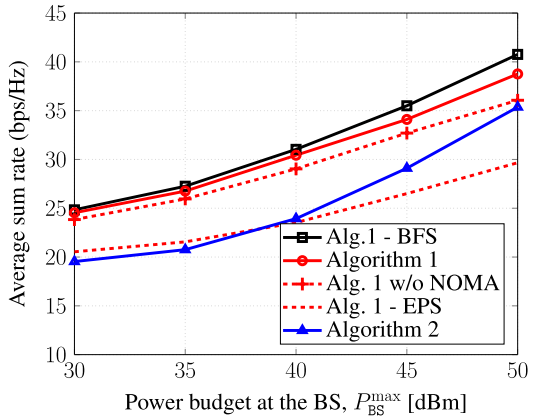

FIGURE 5. Average SR of the considered schemes versus the power budget at the BS, $P_{\mathrm{BS}}^{\max}$ with $N = 8$.

using (15) makes the DCC-based problem inefficient. In addition, the gap between the ACC and DCC in Algorithm 2 is more remarkable, compared to that of Algorithm 1. This is because UE-i in ZFBF-NOMA design has less opportunity to harvest RF power due to ZFBF constraints that results in a low amplitude of the rectified voltage, thereby restricting its computational capability. This confirms the effectiveness of using ACC, and thus it will be used for performance comparison in the following simulations.

In Fig. 5, we plot the average SR performance of the considered schemes as a function of the power budget at the BS, $P_{\mathrm{BS}}^{\max}$ with $N = 8$. For the EPS-based Algorithm 1 and Algorithm 2, their initial feasible points may not be found at a small level of $P_{\mathrm{BS}}^{\max}$ for some channel realizations. As a result, the performance of those infeasible channels is set as zero. As can be seen, the average SR of all considered schemes is monotonically increasing with respect to $P_{\mathrm{BS}}^{\max}$. For a larger value of $P_{\mathrm{BS}}^{\max}$, it is reasonable to exploit the desired signal to fulfill the requirement of the ACC power consumption and harvested DC power since it also improves the achievable rate. As expected, the BFS-based scheme provides the best SR among all considered schemes, especially when $P_{\mathrm{BS}}^{\max}$ increases. A high transmit power results in a strong network

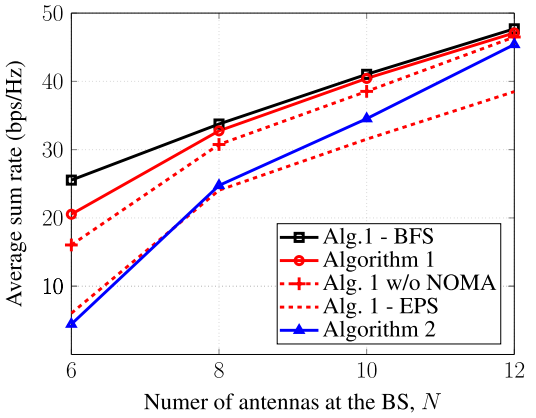

FIGURE 6. Average SR of the considered schemes versus the number of antennas at the BS, N with $P_{\mathrm{BS}}^{\max} = 42$ dBm.

interference, and thus the optimal user-pairing based on the BFS becomes more efficient. However, we recall that the BFS method requires extremely high complexity, and thus only acts as an upper bound for our proposed schemes. Furthermore, the SRs for the other baseline schemes show a performance degradation compared to the proposed Algorithm 1, which confirm the advantages of using NOMA transmission and jointly optimizing power slitting coefficients. With the increase in $P_{\mathrm{BS}}^{\max}$, near users in the EPS-based scheme may be allocated more harvested power than their need. This results in a resource allocation mismatch, leading to a poor performance of the EPS-based scheme. The SR of Algorithm 2 (ZFBF-NOMA) increases dramatically when $P_{\mathrm{BS}}^{\max} >$ 40 dBm and approaches that of Algorithm 1 without NOMA at $P_{\mathrm{BS}}^{\max} = 50$ dBm due to free of interference.

In Fig. 6, we show the average SR versus the number of antennas equipped at the BS with $P_{\mathrm{BS}}^{\max} = 42$ dBm. It is observed that when the number of antennas increases, the SR is substantially increased for all solutions. These results are probably attributed to the fact that, by increasing the number of antennas, more degrees of freedom are added to the system, leading to more efficient resource utilization. Again, the proposed Algorithm 1 provides a substantial performance gain compared to the other baseline schemes. For small N (i.e., $N < 8$), the gap between Algorithm 1 with and without NOMA is remarkable due to a lack of degrees of freedom, revealing the importance of using NOMA transmission in severe network interference. Another interesting observation is that, Algorithm 2 with ZFBF-NOMA results in much lower SR than Algorithm 1 at $N = 6$, owing to the interference-free conditions (recall the total number of users is 6). When N increases, the effect of interference-free conditions (or ZF constraints) becomes less, and Algorithm 2 achieves closer SR to Algorithm 1.

In the last simulation result, we plot a trade-off between the SR and individual harvested DC power requirement, $\bar{P}^{\mathrm{DC}} \equiv \bar{P}_i^{\mathrm{DC}}, \forall i \in \mathcal{K}_{\mathrm{I}}$ with $N = 12$ and $P_{\mathrm{BS}}^{\max} = 42$ dBm. This is accomplished by varying $\bar{P}^{\mathrm{DC}}$ in (14d) over the range $[-30, 0]$ dBm, and the result is shown in Fig. 7. An expected observation from the figure is that the SR-harvested DC power

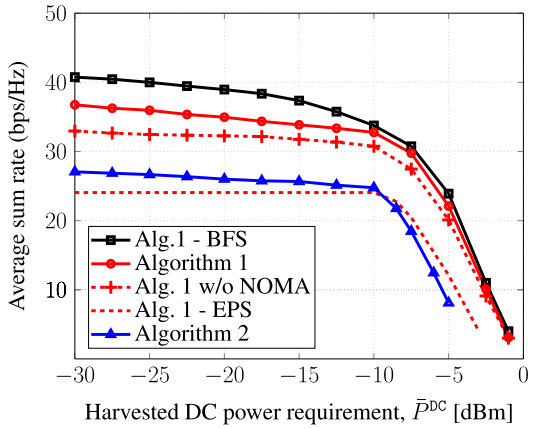

FIGURE 7. Trade-off between the total sum rate and individual harvested DC power requirement, $\bar{P}^{\mathrm{DC}} \equiv \bar{P}_i^{\mathrm{DC}}, \forall i \in \mathcal{K}_{\mathrm{I}}$ with $N = 12$ and $P_{\mathrm{BS}}^{\max} = 42$ dBm.

regions shrink when $\bar{P}^{\mathrm{DC}}$ increases. Specifically, the SR of all schemes is degraded with respect to the individual harvested DC power requirement $\bar{P}^{\mathrm{DC}}$, and it is even more dramatic when $\bar{P}^{\mathrm{DC}} \geq -10$ dBm. For small $\bar{P}^{\mathrm{DC}}$, a small portion of the received signal already fulfills the harvested DC power requirement, and thus the BS mainly allocates the power to the ID receivers. However, when the harvested DC power requirement becomes more stringent, more power needs to be allocated to the EH receivers to make (14d) feasible, which in turn results in low reception power at the ID receivers. We also observe that Algorithm 1 with and without NOMA achieve closer performance to Algorithm 1 with BFS as $\bar{P}^{\mathrm{DC}} \geq -5$ dBm. This phenomenon can be explained as follows: For high $\bar{P}^{\mathrm{DC}}$, the BS has to align the transmit signals around near users in inner-zone to fulfill this need, and thus the SR of all users is mainly contributed by these users. In other words, the use of BFS is not crucial for the design when the requirement of $\bar{P}^{\mathrm{DC}}$ becomes extremely stringent, which also supports our statement made in Remark 3. In addition, compared with Algorithm 1 with EPS, Algorithm 2 is able to achieve better SR for reasonable operational regions, but its maximal harvested DC power ability is inferior to Algorithm 1 with EPS. This is because in the former the interference signal, which can be used to boost the harvested DC power, is partially canceled by ZFBF-NOMA, while the latter aims to balance the signals received at the ID and EH receivers.

VII. CONCLUSION

In this paper, we have proposed an efficient NOMA-assisted MISO-SWIPT system under a practical nonlinear EH circuit, where the PS protocol is adopted at the near users to realize both wireless RF-EH and information decoding. To improve the efficiency of the EH power, an AC computing is adopted to directly supply the wirelessly harvested AC power for the ACC logic without rectification and regulation. We have investigated the problem of SR maximization under QoS requirement for individual user, EH constraints at near users and power constraint at the BS, by jointly optimizing the beamformers and PS ratios. To efficiently solve the nonconvex problem design, we have transformed it into an equivalent nonconvex, but more tractable, one and then proposed an IA-based algorithm for its solution, where the convex problem solved at each iteration can be cast as an SOCP. The proposed algorithm is provably convergent at least to local optima. In addition, for a lower-complexity design, we have proposed the zero-forcing beamforming-based NOMA and customized the IA-based algorithm to solve the problem. Numerical results have been provided to demonstrate the advantages of our proposed approaches. Specifically, the observations have confirmed the efficacy of the proposed NOMA transmission with AC computing in improving system performance, compared to the baseline schemes. Although the performance of the proposed method based on a random user-pairing approaches that of Brute-Force Search method in some extreme cases, it is desirable to investigate an optimal user-pairing with much lower complexity, and thus will be reported in the follow-up work.

REFERENCES

[1] (Mar. 2017). *Cisco Visual Networking Index: Global Mobile Data Traffic Forecast Update, 2016–2021*. [Online]. Available: https://www.cisco.com/c/en/us/solutions/collateral/service-provider/visual-networking-index-vni/mobile-white-paper-c11-520862.html

[2] Z. Ding, Y. Liu, J. Choi, Q. Sun, M. Elkashlan, C.-L. I, and H. V. Poor, "Application of non-orthogonal multiple access in LTE and 5G networks," *IEEE Commun. Mag.*, vol. 55, no. 2, pp. 185–191, Feb. 2017.

[3] S. M. R. Islam, N. Avazov, O. A. Dobre, and K.-S. Kwak, "Power-domain non-orthogonal multiple access (NOMA) in 5G systems: Potentials and challenges," *IEEE Commun. Surveys Tuts.*, vol. 19, no. 2, pp. 721–742, 2nd Quart., 2017.

[4] Y. Liu, Z. Qin, M. Elkashlan, Z. Ding, A. Nallanathan, and L. Hanzo, "Nonorthogonal multiple access for 5G and beyond," *Proc. IEEE*, vol. 105, no. 12, pp. 2347–2381, Dec. 2017.

[5] Y. Saito, Y. Kishiyama, A. Benjebbour, T. Nakamura, A. Li, and K. Higuchi, "Non-orthogonal multiple access (NOMA) for cellular future radio access," in *Proc. IEEE Veh. Technol. Conf. (VTC Spring)*, Jun. 2013, pp. 1–5.

[6] Z. Ding, R. Schober, and H. V. Poor, "A general MIMO framework for NOMA downlink and uplink transmission based on signal alignment," *IEEE Trans. Wireless Commun.*, vol. 15, no. 6, pp. 4454–4483, Jun. 2016.

[7] V. D. Nguyen, H. D. Tuan, T. Q. Duong, H. V. Poor, and O.-S. Shin, "Precoder design for signal superposition in MIMO-NOMA multicell networks," *IEEE J. Sel. Areas Commun.*, vol. 35, no. 12, pp. 2681–2695, Dec. 2017.

[8] Z. Ding, P. Fan, and H. V. Poor, "Impact of user pairing on 5G nonorthogonal multiple-access downlink transmissions," *IEEE Trans. Veh. Technol.*, vol. 65, no. 8, pp. 6010–6023, Aug. 2016.

[9] M. S. Ali, H. Tabassum, and E. Hossain, "Dynamic user clustering and power allocation for uplink and downlink non-orthogonal multiple access (NOMA) systems," *IEEE Access*, vol. 4, pp. 6325–6343, 2016.

[10] X. Lu, P. Wang, D. Niyato, D. I. Kim, and Z. Han, "Wireless networks with RF energy harvesting: A contemporary survey," *IEEE Commun. Surveys Tuts.*, vol. 17, no. 2, pp. 757–789, 2nd Quart., 2015.

[11] I. Krikidis, S. Timotheou, S. Nikolaou, G. Zheng, D. W. K. Ng, and R. Schober, "Simultaneous wireless information and power transfer in modern communication systems," *IEEE Commun. Mag.*, vol. 52, no. 11, pp. 104–110, Nov. 2014.

[12] M.-L. Ku, W. Li, Y. Chen, and K. J. R. Liu, "Advances in energy harvesting communications: Past, present, and future challenges," *IEEE Commun. Surveys Tuts.*, vol. 18, no. 2, pp. 1384–1412, 2nd Quart. 2016.

[13] C. R. Valenta and G. D. Durgin, "Harvesting wireless power: Survey of energy-harvester conversion efficiency in far-field, wireless power transfer systems," *IEEE Microw. Mag.*, vol. 15, no. 4, pp. 108–120, Jun. 2014.

[14] T. Le, K. Mayaram, and T. Fiez, "Efficient far-field radio frequency energy harvesting for passively powered sensor networks," *IEEE J. Solid-State Circuits*, vol. 43, no. 5, pp. 1287–1302, May 2008.

[15] Q. Shi, L. Liu, W. Xu, and R. Zhang, "Joint transmit beamforming and receive power splitting for MISO SWIPT systems," *IEEE Trans. Wireless Commun.*, vol. 13, no. 6, pp. 3269–3280, Jun. 2014.

[16] R. Zhang and C. K. Ho, "MIMO broadcasting for simultaneous wireless information and power transfer," *IEEE Trans. Wireless Commun.*, vol. 12, no. 5, pp. 1989–2001, May 2013.

[17] D. W. K. Ng, E. S. Lo, and R. Schober, "Robust beamforming for secure communication in systems with wireless information and power transfer," *IEEE Trans. Wireless Commun.*, vol. 13, no. 8, pp. 4599–4615, Aug. 2014.

[18] E. Boshkovska, D. W. K. Ng, N. Zlatanov, A. Koelpin, and R. Schober, "Robust resource allocation for MIMO wireless powered communication networks based on a non-linear EH model," *IEEE Trans. Commun.*, vol. 65, no. 5, pp. 1984–1999, May 2017.

[19] K. Xiong, B. Wang, and K. J. R. Liu, "Rate-energy region of SWIPT for MIMO broadcasting under nonlinear energy harvesting model," *IEEE Trans. Wireless Commun.*, vol. 16, no. 8, pp. 5147–5161, Aug. 2017.

[20] J.-M. Kang, I.-M. Kim, and D. I. Kim, "Wireless information and power transfer: Rate-energy tradeoff for nonlinear energy harvesting," *IEEE Trans. Wireless Commun.*, vol. 17, no. 3, pp. 1966–1981, Mar. 2018.

[21] J. Choi, "Minimum power multicast beamforming with superposition coding for multiresolution broadcast and application to NOMA systems," *IEEE Trans. Commun.*, vol. 63, no. 3, pp. 791–800, Mar. 2015.

[22] Z. Chen, Z. Ding, X. Dai, and G. K. Karagiannidis, "On the application of quasi-degradation to MISO-NOMA downlink," *IEEE Trans. Signal Process.*, vol. 64, no. 23, pp. 6174–6189, Dec. 2016.

[23] Z. Chen, Z. Ding, and X. Dai, "Beamforming for combating inter-cluster and intra-cluster interference in hybrid NOMA systems," *IEEE Access*, vol. 4, pp. 4452–4463, Aug. 2016.

[24] M. F. Hanif, Z. Ding, T. Ratnarajah, and G. K. Karagiannidis, "A minorization-maximization method for optimizing sum rate in the downlink of non-orthogonal multiple access systems," *IEEE Trans. Signal Process.*, vol. 64, no. 1, pp. 76–88, Jan. 2016.

[25] J. Tang, J. Luo, M. Liu, D. K. C. So, E. Alsusa, G. Chen, K.-K. Wong, and J. A. Chambers, "Energy efficiency optimization for NOMA with SWIPT," *IEEE J. Sel. Topics Signal Process.*, vol. 13, no. 3, pp. 452–466, Jun. 2019.

[26] L. Dai, B. Wang, M. Peng, and S. Chen, "Hybrid precoding-based millimeter-wave massive MIMO-NOMA with simultaneous wireless information and power transfer," *IEEE J. Select. Areas Commun.*, vol. 37, no. 1, pp. 131–141, Jan. 2019.

[27] Y. Xu, C. Shen, Z. Ding, X. Sun, S. Yan, G. Zhu, and Z. Zhong, "Joint beamforming and power-splitting control in downlink cooperative SWIPT NOMA systems," *IEEE Trans. Signal Process.*, vol. 65, no. 18, pp. 4874–4886, Sep. 2017.

[28] B. Su, Q. Ni, and W. Yu, "Robust transmit beamforming for SWIPT-enabled cooperative NOMA with channel uncertainties," *IEEE Trans. Commun.*, vol. 67, no. 6, pp. 4381–4392, Jun. 2019. doi: 10.1109/TCOMM.2019.2900318.

[29] Y. Yuan, Y. Xu, Z. Yang, P. Xu, and Z. Ding, "Energy efficiency optimization in full-duplex user-aided cooperative SWIPT NOMA systems," *IEEE Trans. Commun.*, to be published. doi: 10.1109/TCOMM.2019.2914386.

[30] T. Wan, Y. Karimi, M. Stanaćević, and E. Salman, "Perspective paper—Can AC computing be an alternative for wirelessly powered IoT devices?" *IEEE Embedded Syst. Lett.*, vol. 9, no. 1, pp. 13–16, Mar. 2017.

[31] T. Wan, Y. Karimi, M. Stanaćević, and E. Salman, "AC computing methodology for RF-powered IoT devices," *IEEE Trans. Very Large Scale Integr. (VLSI) Syst.*, vol. 27, no. 5, pp. 1017–1028, May 2019.

[32] E. Salman, M. Stanaćević, S. Das, and P. M. Djurić, "Leveraging RF power for intelligent tag networks," in *Proc. Great Lakes Symp. VLSI*, May 2018, pp. 329–334.

[33] V.-D. Nguyen, H. V. Nguyen, O. A. Dobre, and O.-S. Shin, "A new design paradigm for secure full-duplex multiuser systems," *IEEE J. Sel. Areas Commun.*, vol. 36, no. 7, pp. 1480–1498, Jul. 2018.

[34] S. Kim, C. H. Ziesler, and M. C. Papaefthymiou, "Charge-recovery computing on silicon," *IEEE Trans. Comput.*, vol. 54, no. 6, pp. 651–659, Jun. 2005.

[35] A. Beck, A. Ben-Tal, and L. Tetruashvili, "A sequential parametric convex approximation method with applications to nonconvex truss topology design problems," *J. Global Optim.*, vol. 47, no. 1, pp. 29–51, May 2010.

[36] B. R. Marks and G. P. Wright, "A general inner approximation algorithm for nonconvex mathematical programs," *Oper. Res.*, vol. 26, pp. 681–683, Jul. 1978.

[37] V.-D. Nguyen, T. Q. Duong, H. D. Tuan, O.-S. Shin, and H. V. Poor, "Spectral and energy efficiencies in full-duplex wireless information and power transfer," *IEEE Trans. Commun.*, vol. 65, no. 5, pp. 2220–2233, May 2017.

[38] A. Wiesel, Y. C. Eldar, and S. Shamai (Shitz), "Linear precoding via conic optimization for fixed MIMO receivers," *IEEE Trans. Signal Process.*, vol. 54, no. 1, pp. 161–176, Jan. 2006.

[39] MOSEK ApS. (2014). [Online]. Available: https://www.mosek.com

[40] A. Ben-Tal and A. Nemirovski, *Lectures on Modern Convex Optimization* (MPS-SIAM Series on Optimization). Philadelphia, PA, USA: SIAM, 2001.

[41] Q. H. Spencer, A. L. Swindlehurst, and M. Haardt, "Zero-forcing methods for downlink spatial multiplexing in multiuser MIMO channels," *IEEE Trans. Signal Process.*, vol. 52, no. 2, pp. 461–471, Feb. 2004.

[42] J. Guo and X. Zhu, "An improved analytical model for RF-DC conversion efficiency in microwave rectifiers," in *IEEE MTT-S Int. Microw. Symp. Dig.*, Jun. 2012, pp. 1–3.

[43] *Spatial Channel Model for Multiple Input Multiple Output (MIMO) Simulations*, document 3GPP TR 25.996, 3rd Generation Partnership Project, 2011. [Online]. Available: http://www.3gpp.org/technologies

[44] J. Lofberg, "YALMIP: A toolbox for modeling and optimization in MATLAB," in *Proc. IEEE Int. Symp. Comput. Aided Control Syst. Design*, Sep. 2004, pp. 284–289.

[45] K. C. Toh, M. J. Todd, and R. H. Tütüncü, "SDPT3—A MATLAB software package for semidefinite programming, version 1.3," *Optim. Methods Softw.*, vol. 11, pp. 545–581, Jan. 1999.

VAN-DINH NGUYEN (S'14) received the B.E. degree in electrical engineering from the Ho Chi Minh City University of Technology, Vietnam, in 2012, and the M.E. and Ph.D. degrees in electronic engineering from Soongsil University, Seoul, South Korea, in 2015 and 2018, respectively. He was a Postdoctoral Visiting Scholar with the University of Technology Sydney, Australia, in 2018, and a Ph.D. Visiting Scholar with Queen's University Belfast, U.K., from 2015 to 2016. From 2012 to 2013, he spent 12 months with Vietnam Television as a Principal Engineer. He is currently a Postdoctoral Researcher and a Lecturer with the School of Electronic Engineering, Department of ICMC Convergence Technology, Soongsil University. He has authored or coauthored some 30 papers published in international journals and conference proceedings. His current research interests include mathematical modeling of 5G cellular networks and machine learning for wireless communications. He has also been a Technical Programme Committee Member for several flagship international conferences in the related fields. He received several best conference paper awards, such as the IEEE TRANSACTION ON COMMUNICATIONS Exemplary Reviewer Award, in 2018, and the IEEE GLOBECOM Student Travel Grant Award, in 2017. He has served as a reviewer for many top-tier international journals on wireless communications. He is an Editor of the IEEE COMMUNICATIONS LETTERS.

OH-SOON SHIN (S'00–M'10) received the B.S., M.S., and Ph.D. degrees from Seoul National University, Seoul, South Korea, in 1998, 2000, and 2004, respectively, all in electrical engineering and computer science. From 2004 to 2005, he was with the Division of Engineering and Applied Sciences, Harvard University, MA, USA, as a Postdoctoral Fellow. From 2006 to 2007, he was a Senior Engineer with Samsung Electronics, Suwon, South Korea. In 2007, he joined the School of Electronic Engineering, Soongsil University, Seoul, where he is currently a Professor. His research interests include communication theory, wireless communication systems, and signal processing for communication.